Available online at www.sciencedirect.com

SciVerse ScienceDirect

Ceramics International 38 (2012) 5007–5014

CERAMICS INTERNATIONAL

www.elsevier.com/locate/ceramint

Enhancement of fracture toughness in bioactive glass-based nanocomposites with nanocrystalline forsterite as advanced biomaterials for bone tissue engineering applications

Abolfazl Yazdanpanah [a], Reza Kamalian [a], Fathollah Moztarzadeh [a], Masoud Mozafari [a,b,*], Roya Ravarian [c], Lobat Tayebi [b]

[a] Biomaterials Group, Faculty of Biomedical Engineering (Center of Excellence), Amirkabir University of Technology, P.O. Box 15875-4413, Tehran, Iran
[b] Helmerich Advanced Technology Research Center, School of Material Science and Engineering, Oklahoma State University, OK 74106, USA
[c] School of Chemical and Biomolecular Engineering, The University of Sydney, New South Wales, NSW 2006, Australia

Received 23 January 2012; received in revised form 24 February 2012; accepted 29 February 2012
Available online 7 March 2012

Abstract

In this research, the replacement effects of bioactive glass (BG) by nanocrystalline forsterite (NF) on the biomineralization, microstructural and mechanical properties of BG-based nanocomposites were investigated. The hybrid nanocomposites with different NF contents (0, 10, 20, and 30 wt%) were prepared from the nanopowders by means of conventional cold pressing method. Surprisingly, the addition of NF provided redundant mechanisms to improve the toughness of the BG matrix without deteriorating its biomineralization properties. In addition, the resulting enhancement in the fracture toughness, observed for the first time in highly bioactive BG/NF nanocomposites, indicated the potential of the prepared nanocomposites as advanced biomaterials for load-bearing bone tissue engineering applications.

Keywords: B. Nanocomposite; C. Mechanical properties; Bioactive glass; Nanocrystalline forsterite

1. Introduction

Different concepts for microstructure design of composites have been proposed to overcome the inherent brittleness of ceramics [1] but most of the predicted improvements have not been achieved. In the range of ceramic materials, and according to their nanostructure, bioactive glasses (BGs) are placed at the farthest end from the conventional ceramics [2]. BGs have been introduced and defined by Hench [3] as materials capable to create a chemical bond with surrounding tissues. BGs in contact with biological environments develop reactive layers at their surfaces resulting in a chemical bond between implant and host tissue [4]. The high reactivity of these materials is the main advantage of their application in periodontal repair and bone augmentation [5–7].

BGs can be obtained by melting method around 1350 °C or by sol–gel method at room temperature [8,9]. There are several advantages of sol–gel-derived BGs over melt-derived ones. Specially, the synthetic route and lower heating temperature lead to increase the numbers of silanol groups and mesopores, both of which act as nucleation sites for apatite formation. Some other merits of this technique are as follow: lower temperature processing, higher bioactivity, interconnected nanometer pores which are able to be impregnated with biologically active phases, no requirement of sodium oxide, higher SiO_2 content (up to 90 mol%). As silica is responsible for network formation, it constitutes the basic component of the BGs. Hence, larger amount of SiO_2 results in more bioactive and stable BGs.

The formation of bone-like apatite occurs not only *in vivo* but also outside the body when BGs are soaked in solutions emulating human plasma. *In vitro* evaluations are applied to predict the behaviour of BGs inside the human body. It has been used to make meaningful connection between biomineralization of apatite *in vitro* and the bone bonding ability to induce

* Corresponding author at: Helmerich Advanced Technology Research Center, School of Material Science and Engineering, Oklahoma State University, OK 74106, USA. Tel.: +1 918 594 8634, fax: +1 270 897 1179.
E-mail address: masoud.mozafari@okstate.edu (M. Mozafari).

0272-8842/$36.00
doi:10.1016/j.ceramint.2012.02.097

bone remodeling *in vivo* [10–12]. The nucleation and growth mechanism of bone-like apatite was proposed for the first time by Kokubo [13]. This mechanism consists of the interchange between Ca^{2+} ions of BG and the H_3O^+ of simulated body fluid (SBF) solution. In turn this causes the formation of Si–OH groups on the BG surface and induces nucleation and growth of apatite. In this context, numerous studies have been done on the glasses obtained by sol–gel method. They belong to different systems such as $CaO–P_2O_5–SiO_2$. These assays revealed that the immersion of BG in SBF increases Ca^{2+} concentration and pH due to the partial dissolution of silica network. Obviously, these changes affect the rate of apatite formation and bone-implant integration.

In another point of view, BGs exhibit osteoconductive properties defined as the characteristic of bone growth in porosities and bonding along the surface. They are also resorbable due to their mineral composition containing calcium and phosphorus similar to natural bone [7]. Their disadvantage lies in their low mechanical strength which limits their applications. Toughening is often an important property required for BGs and glass-ceramics. Also, for long-term implants, it may be important to increase the toughness as much as possible without losing bioactivity.

In recent years, some Si and Mg containing bioceramics have drawn interests in the development of bone implant materials [14]. Nanocrystalline forsterite (NF) is one of these bioceramic materials. Compared with most of ceramics, NF showed a significant improvement in the fracture toughness about which superior to the lower limit reported for bone implant [15]. In addition, Ni et al. [16] showed that NF is a novel bioceramic with high mechanical properties and good biocompatibility and could be suitable for hard tissue repair in load-bearing sites. In addition, the nanometer-sized grains and the high volume fraction of grain boundaries in nanostructured materials are reported to show improved biocompatibility over normal materials [17–19], and increased osteoblast adhesion and proliferation [20]. According to the above points, NF bioceramic is expected to have better mechanical properties than BG, and the addition of NF can improve the mechanical properties of the implants needed for bone defect repairing.

In this research, the nanocomposites were prepared from nanopowder with different amount of NF to study their effects on the mechanical properties and surface reactivity of the samples.

2. Materials and methods

2.1. Preparation of BG

The BG consisting of 64%SiO_2, 5%P_2O_5, and 31%CaO (mol%) was synthesized as follows: 14.8 g (0.064 mol) of tetraethylorthosilicate (TEOS) was added into 30 ml of 0.1 M nitric acid, the mixture was allowed to react for 30 min for the acid hydrolysis of TEOS to proceed almost to completion. The following reagents were added in sequence allowing 45 min for each reagent to react completely: 0.85 g (0.005 mol) triethyl phosphate (TEP), and 7.75 g (0.031 mol) of calcium nitrate tetrahydrate. After the final addition, mixing was continued for 1 h to allow completion of the hydrolysis reaction. The solution was cast in a cylindrical Teflon container and kept sealed for 10 days at room temperature to allow the hydrolysis and a polycondensation reaction to take place until the gel was formed. The gel was kept in a sealed container and heated at 70 °C for an additional 3 days. The water was removed and a small hole was inserted in the lid to allow the leakage of gases while heating the gel to 120 °C for 2 days to remove all the water. Subsequently, the powder was milled for 10 h by planetary mill (SVD15IG5-1, LG Company).

2.2. Preparation of NF

Briefly, a transparent sol was prepared by dissolving 0.0142 mol magnesium nitrate (3.639 g) in 50 ml of de-ionized water. Next, 0.0071 mol of silica (1.642 g of colloidal silica) was introduced into the solution to set MgO/SiO_2 molar ratio to 2:1 which corresponds to the theoretical value of pure NF. As the second solution which was prepared separately, 0.0568 mol (19.426 g) sucrose was added into 100 ml of de-ionized water. Then, two solutions were mixed together and continuously stirred for 2 h. In the next step, 0.0071 mol (0.312 g) of PVA was mixed with 20 ml of de-ionized water to prepare a PVA solution and then was added into the final solution and pH was adjusted to 1 by drop-wise addition an appropriate amount of diluted nitric acid, and finally the mixture stirred for 4 h. Here, the mole ratio of the Mg^{2+} ions, sucrose and PVA monomer was 1:4:0.5. With the aim of letting the Mg^{2+} ions to react with sucrose completely the solution heated at 80 °C for 2 h on a hot plate stirrer, and then heated in an electric oven at 200 °C for complete dehydration and changing into a viscous dark brownish gel. Subsequently, the obtained mass was milled into fine powder by planetary milling. After grinding and sieving, the dry powder calcined for 3 h at 900 °C.

2.3. Preparation of BG/NF nanocomposites

The synthesized BG powder was mixed with different ratios of the synthesized NF as listed in Table 1, to prepare BG/NF nanocomposite samples. Four mixtures of BG/NF, with various weight ratios, were prepared in a planetary ball mil (Retch PMA, Brinkman, USA) for 30 min to ensure homogeneity. Next, each batch was carefully mixed with about 0.1 wt% of carboxymethyl cellulose (CMC) as an appropriate binding agent. Then, the mixtures were formed to disks using cold press molding method. Green compact disks were achieved by using a predetermined amount of mixed powder, which resulted in the targeted thickness (about 15 mm) after being pressed uniaxially in a steel die of 13 mm in diameter under the pressure of 50 MPa. Finally, composites were sintered at 1000 °C for 2 h.

2.4. Preparation of SBF solution

The SBF solution was prepared by dissolving reagent-grade NaCl, KCl, $NaHCO_3$, $MgCl_2·6H_2O$, $CaCl_2$ and KH_2PO_4 into distilled water and buffered at pH = 7.25 with TRIS

Table 1
The component of the BG/NF nanocomposite samples.

Sample	BG (wt%)	NF (wt%)
NC0	100	0
NC1	90	10
NC2	80	20
NC3	70	30

(trishydroxymethyl aminomethane) and 1 N HCl solution at 37 °C. Its composition is given in Table 2 and is compared with the human blood plasma. It should be also noted that SBF is a solution highly supersaturated with respect to apatite.

2.5. Sample characterization

Transmission electron microscopy (TEM) study was performed with the Philips CM120 operated at 100 kV. For TEM analysis, the nanoparticles were ultrasonically dispersed in ethanol for 15 min to form very dilute suspensions, and then few drops were deposited on the carbon-coated copper grids.

The microstructures of the samples were evaluated using scanning electron microscopy (SEM). The samples were coated with a thin layer of Gold (Au) by sputtering (EMITECH K450X, England) and then the morphology of them were observed on a scanning electron microscope (SEM-Philips XL30) that operated at the acceleration voltage of 15 kV. Also, Energy dispersive X-ray analyzer (EDX) (Rontec, Germany) connected to SEM was used to investigate semi-quantitatively chemical compositions.

The samples were characterized using FTIR with Bomem MB 100 spectrometer. For IR analysis, 1 mg of the scraped samples were carefully mixed with 300 mg of KBr (infrared grade) and palletized under vacuum. Then, the pellets were analyzed in the range of 400–4000 cm^{-1} with 4 cm^{-1} resolution averaging 120 scans.

The samples were analyzed by X-ray diffraction (XRD) with Siemens-Brucker D5000 diffractometer. This instrument works with voltage and current settings of 40 kV and 40 mA respectively and uses Cu-Kα radiation (1.540600 Å). For qualitative analysis, XRD diagrams were recorded in the interval $10^\circ \leq 2\theta \leq 50^\circ$at scan speed of 2°/min.

Mechanical behavior of the prepared nanocomposite samples was investigated by using compression strength test.

Table 2
Ion concentrations of simulated body fluid (SBF) and human blood plasma.

Ion	Plasma (mmol/l)	SBF (mmol/l)
Na^+	142.0	142.0
K^+	5.0	5.0
Mg^{+2}	1.5	1.5
Ca^{+2}	2.5	2.5
Cl^-	103.0	147.8
HCO_3^-	27	4.2
HPO_4^{-2}	1.0	1.0
SO_4^{-2}	0.5	0.5

The cylindrical specimens were prepared to an appropriate size (13 mm in diameter and 15 mm in thickness), and the thicknesses were measured with an electric digital caliper. Then, the compressive strengths of the wet samples were measured by a Zwick/Roell Universal Testing Machine apparatus with a crosshead speed of 1 mm/min. The following equations were used for the calculation of E (elastic constant) (1) [21,22] and σ (yield stress) (2):

$$E = \frac{KL}{A} \tag{1}$$

$$\sigma = \frac{F}{A} \tag{2}$$

where F = ultimate load; K = stiffness; L = length of sample; A = average of surface area calculated from the following equation (3):

$$A = \frac{\pi}{2} \times \frac{1}{4(d_1^2 + d_1^2)} \tag{3}$$

where d_1 and d_2 are the diameters of the bases of the cylindrical samples. The fracture toughness of the samples was obtained from the area under the stress–strain curve normalized by the specimen's surface area.

2.6. In vitro biomineralization study

SBF *in vitro* method has often been used in the biomineralization evaluation of bioactive materials as a quick, easy and cost effective method. SBF is a good simulation of the osteoproduction environment in osseous tissue and has been proved to be an efficient technique to study the bioactivity of biomaterials and the mechanism of bone bonding. However, SBF is not a certain method to investigate the osteoinduction of biomaterials, and the results from SBF may not be consistent with the *in vivo* results in a real condition. The local ion concentration is the key factor to affect the formation of apatite. The effect of body fluid flowing on local ion concentration could not be ignored during the *in vivo tests*. That explains why recently investigators are trying to simulate the body environment by using dynamic protocols. In this way they not only simulate the ion concentration of body fluid, but also simulate the effect of body fluid flowing on the local ion concentration near the surface of biomaterials in body environment. It seems that such dynamic SBF tests would preferably simulate the osteoinduction environment and would be used in osteoinductivity evaluation of bioceramics.

Here, we carried out an *in vitro* study by soaking the nanocomposite samples in SBF solution with concentration of 1 mg sample per milliliter of the fluid at 37 °C for 14 days. At regular intervals (1, 3, 7, 14 days) samples were taken out and rinsed with doubly distilled water, and dried in an oven at 40 °C for 10 h before analysis by SEM and EDX. For this purpose, the samples were covered with a thin film of Au (to avoid charges accumulation at the surface of the analyzed materials) after immersion in SBF. In our study, the SBF was not renewed

during the experiment, as a previously described static protocol [23,24].

2.7. Statistical analysis

All experiments were performed in fifth replicate. The results were given as means ± standard error (SE). Statistical analysis was performed by using One-way ANOVA and Tukey test with significance reported when $P < 0.05$. Also for investigation of group normalizing, Kolmogorov–Smirnov test was used.

3. Results and discussion

3.1. TEM observations of NF particles

TEM as a powerful tool for observing the morphology and size of nanoparticles was used to determine the obtained morphology and nano size of the synthesized single-phase NF. Fig. 1 shows the TEM micrograph of the NF particles after the final heat-treatment process. The micrograph indicated that the particles were nearly elliptical shaped morphology and the size was in the range of 10–50 nm. It is important to point out that the nanostructured ceramics have superior mechanical properties [15]. In addition, the nanometer-sized grains and the high volume fraction of grain boundaries in nanostructured materials are reported to show improved biocompatibility over normal materials, and increased osteoblast adhesion and proliferation. According to the above points, nanostructured NF bioceramic is expected to have even better mechanical properties and biocompatibility than coarser crystals. It was reported that coarse grain NF had an extremely low degradation rate and was not that bioactive [15]. Recent studies in this field [25] indicated that NF nanopowder, unlike micron-sized forsterite, possessed apatite-formation ability. The bioactivity of the NF when compared to coarse grain forsterite shows a greater effect of the nanophase forsterite on its ion dissolution in biological solution [26].

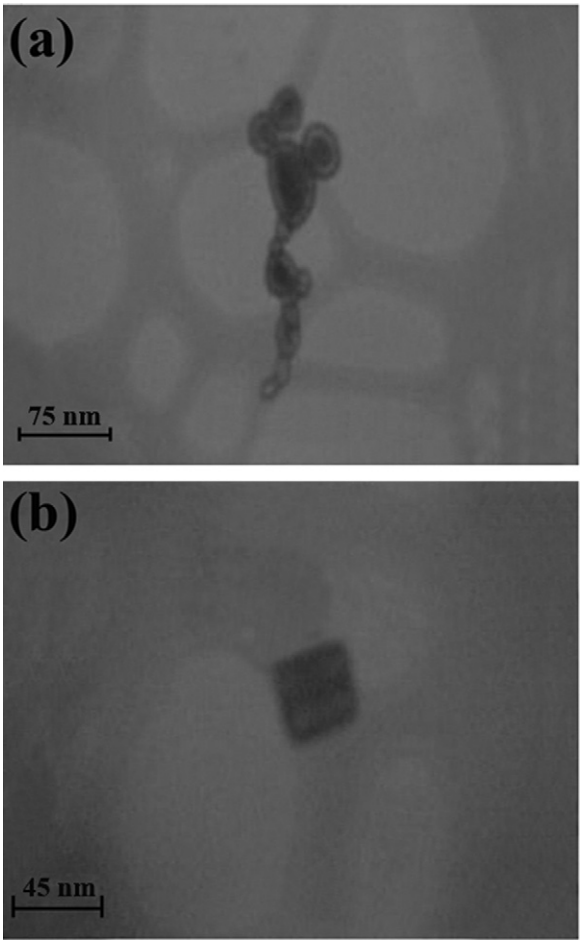

Fig. 1. TEM micrographs of the synthesized NF particles.

3.2. Microstructural properties of BG/NF nanocomposites

The XRD patterns of the BG/NF nanocomposite samples with different percentages of BG and NF (NC1, NC2 and NC3) are shown in Fig. 2. It can be concluded from this figure that the main phases of the nanocomposite samples are NF and pseudowollastonite. According to the JCPDS data file No. 34-0189, all the characteristic peaks of NF phase were obviously

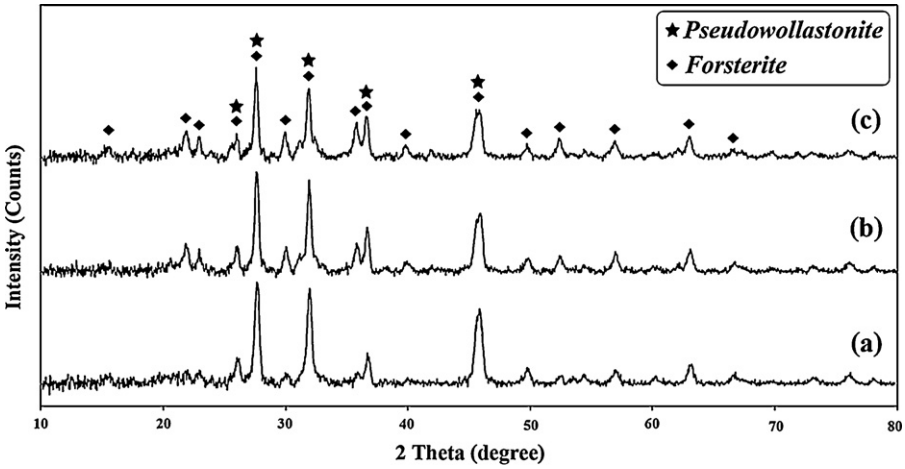

Fig. 2. The XRD patterns of the BG/NF nanocomposite samples with different percentages of nBG and nF: (a) NC1, (b) NC2 and (c) NC3.

detected. The XRD analysis also showed some small peaks which may be related to the formation of a small amount of enstatite (according to JCPDS data file No. 11-0273) along with NF at higher temperatures. In addition, regarding to the XRD patterns, it can be concluded that at temperatures higher than 700 °C, α-TCP and pseudowollastonite (JCPDS data file No. 19-0248) have started to crystallize and at 1000 °C these two phases partly crystallized. Also, the obtained results are similar to the previous studies [27].

It is worth mentioning that the pseudowollastonite phase is a highly bioactive material that induces direct bone growth, and its *in vitro* and *in vivo* tests have been fully investigated [28]. With comparing the intensity of the formed phases, it can be obviously concluded that sample NC1 has the most content of pseudowollastonite and sample NC3 has the least content of pseudowollastonite or it can be said that it has the most content of NF phase.

3.3. Mechanical properties

Generally, an ideal tissue engineering implant made from bioceramics should be biocompatible and highly porous with adequate mechanical properties. For this purpose the prepared nanocomposites were tested to determine the effects of using the NF phase on the mechanical properties of the BG-based nanocomposite samples. According to the previous explanations, as NF ceramics showed a significant improvement in the fracture toughness superior to the lower limit reported for bone implant, they can be used as alternative bioactive ceramic materials as a component of nanocomposites with the aim of enhancing in the toughening properties. Since that the fracture toughness of different materials can be modified by adjusting the NF content, the influence of changing the overall NF content on the fracture toughness was investigated for the prepared nanocomposite samples. The Elastic modulus, yield stress and fracture toughness of the nanocomposites are graphically illustrated in Fig. 3(a)–(c), respectively.

The obtained results, given in this figure, clearly revealed that the fracture toughness of the nanocomposites increased with increasing the NF content from 10 to 30 wt%. An acceptable fracture toughness of 0.22 MPa $m^{1/2}$ was obtained for the NC3 sample. The yield stress of the nanocomposites was also influenced by the addition of the NF content down to 4.3 MPa for NC3 sample, whereas the Elastic modulus decreased with increasing the NF content. The Elastic modulus of the nanocomposites was strongly influenced by the NF content and decreased with increasing the NF content from 490 MPa for the NC0 up to 110 MPa for the NC3 sample.

3.4. Sample characterization after in vitro assays in SBF

The essential condition for biomaterials to bond with living bone is the formation of a surface apatite layer in the body environment [20]. To determine the bioactivity of these materials, the prepared nanocomposite samples were subjected to *in vitro* testing using SBF solution. The samples were immersed in SBF at 37 °C for 14 days. Morphological and textural properties of the biomaterials also indicate that soaking in SBF led to the formation of an apatite layer on the surface of the samples. Herein, apatite was incorporated into the surface of the nanocomposites *in situ via* the SBF technique. Fig. 4(a)–(d) shows the SEM micrographs of the nanocomposite samples after immersion for 14 days. According to the observations, scattered and small particles were covered on the surface of the nanocomposites after 14 days of immersion. The whole wall surfaces of the nanocomposites were covered by a layer of

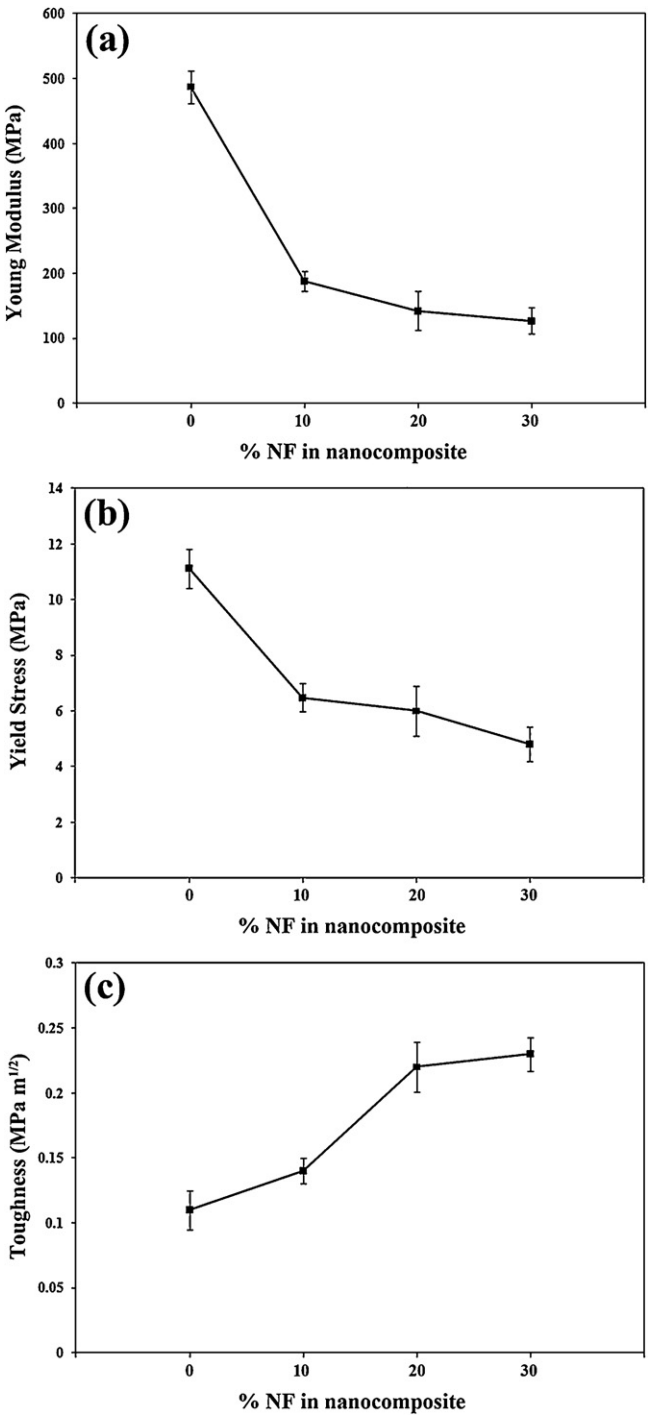

Fig. 3. The mechanical properties of the synthesized nanocomposite samples: (a) elastic modulus, (b) yield stress and (c) fracture toughness.

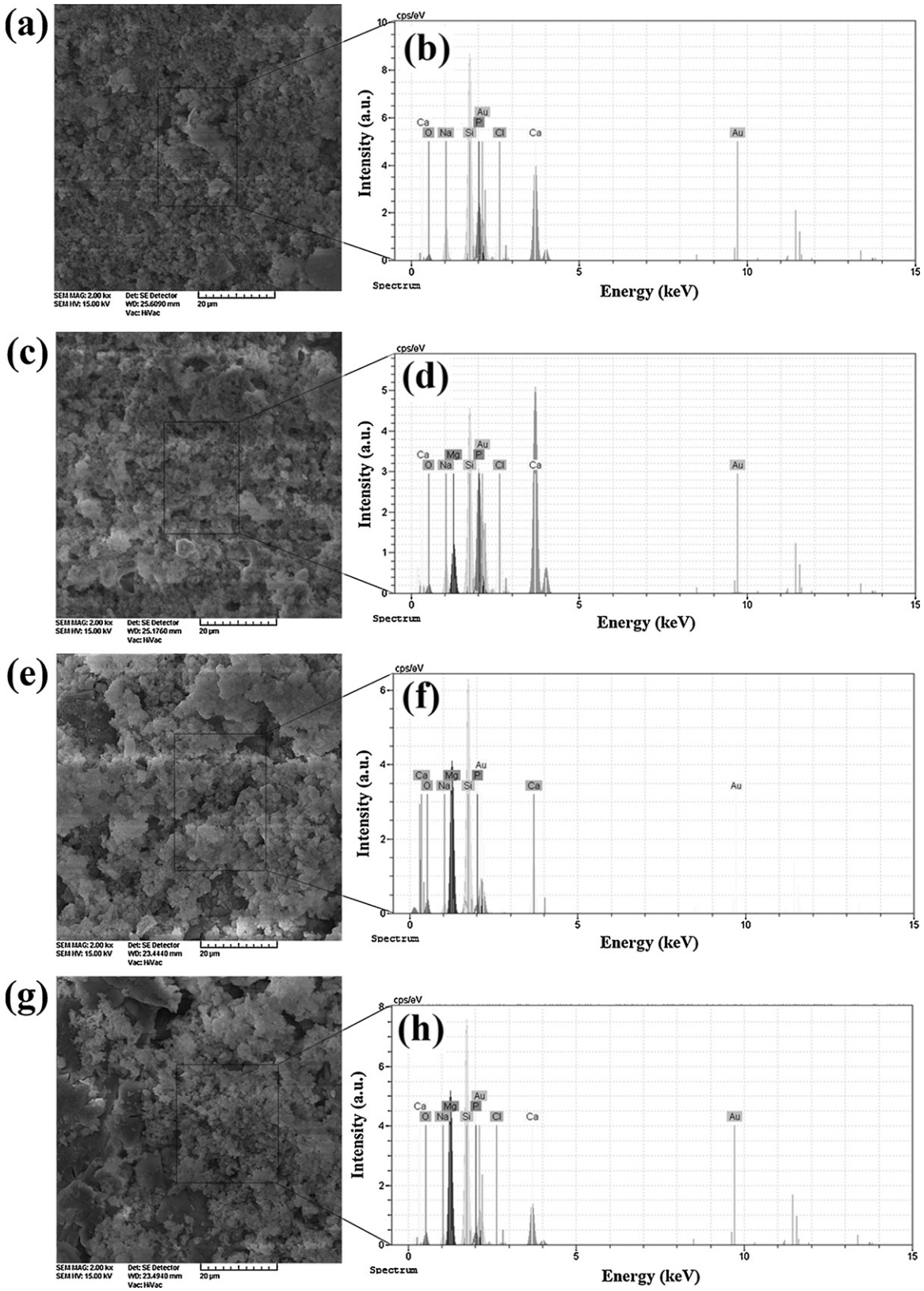

Fig. 4. The SEM-EDX micrographs of the nanocomposite samples after immersion for 14 days: (a) and (b) NC0, (c) and (d) NC1, (e) and (f) NC2, (g) and (h) NC3.

apatite, and the underlying surfaces were not clearly observable and in all of the samples there can be seen the apatite particles which formed on the surfaces after soaking in SBF. According to the observations, addition of NF particles to the BG phase did not significantly change its bioactivity and biocompatibility, and the prepared nanocomposites are still highly bioactive.

We also confirmed the formation of apatite layer on the surface of nanocomposites by EDX analysis, so the apparition of apatite formations on the surfaces of nanocomposite samples after immersion in SBF solution was established by EDX procedure, as revealed by the pictures from Fig. 4. The EDX spectra show all the characteristic peaks of BG and NF phases but the presence of gold (Au) on the surfaces was only related to the sputtering before SEM analysis.

For the first sample (NC0) in SBF solution, EDX analysis showed that the Ca/P ratio was near the stoichiometric apatite which was about 1.69 but for the second sample (NC1) there was an increase in the Ca intensity that caused also the increase of the Si peak due to addition of NF, and the molar ratio of Ca/P developed to a value which was corresponded to nonstoichiometric biological apatite (1.76). The Mg peak also appeared in this pattern due to the addition of 10% NF. In addition, for the sample (NC2) the Ca/P molar ratios improved in the range of 2.52. As it can be seen in the SEM micrographs, the whole surfaces of the nanocomposites were covered by a Ca/P layer which created a dune-like apatite covering. Also, the results from EDX analysis revealed the gradual development of the Ca/P ratio of the apatite layer along with addition of NF powder to the nanocomposite samples after immersion in SBF solution. Furthermore, EDX analysis showed that for samples containing more NF particles (NC3 sample) after 14 days immersion in SBF solution, the Ca/P ratios were in accordance to nonstoichiometric biological apatite which was approximately 3.21.

Fig. 5 shows the FTIR spectra of the prepared samples after 14 days immersion in SBF solution (in the 400–4000 cm^{-1} spectral range). As can be seen, all samples exhibited some infrared bands around 800, 900, 1000 and 1200 cm^{-1} which are attributed to the silicate network. They ascribed to the Si–O symmetric stretching of bridging oxygen atoms between tetrahedrons, Si–O stretching of non-bridging oxygen atoms, Si–O–Si symmetric stretching, and the LO mode (out-of-phase motion of adjacent oxygen atoms) of Si–O–Si asymmetric stretching. The band located around 600 cm^{-1} is attributed to the asymmetric vibration of PO_4^{3-} [29–32]. In addition, the NF containing samples exhibited the main characteristic bands of ideal NF. For instance, the bands related to the characteristic peaks of NF appeared around 488 and 643 cm^{-1} for SiO_4 bending, at 910 and 1092 cm^{-1} for SiO_4 stretching and at 483 cm^{-1} for modes of octahedral MgO_6. In addition, the broad band centered at 3400 cm^{-1} ascribed to O–H band. Our results are in agreement with previous studies [33,34]..

The bands around 870 and 1500 cm^{-1} indicated the presence of CO_3^{2-} groups. The bands observed at 603, 1000 and 1250 cm^{-1} are attributed to P–O bending [19]. Also the spectra are quite similar to HAp. The characteristic bonds exhibited in the sample's spectra assigned here are as follow:

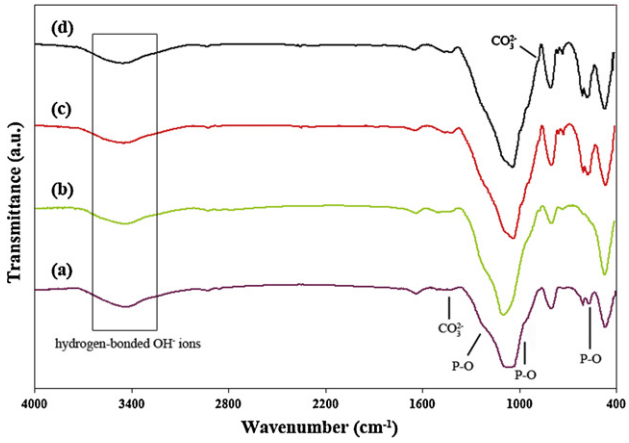

Fig. 5. The FTIR spectra of the nanocomposite samples after immersion for 14 days: (a) NC0, (b) NC1, (c) NC2, (d) NC3.

- Two bonds around 3487 and 613 cm^{-1} were related to the stretching mode of hydrogen-bonded OH^- ions and liberational mode of hydrogen-bonded OH^- ions, respectively.
- The bands around 1000 and 603 cm^{-1} were attributed to υ_3 PO_4 and υ_4 PO_4 respectively.

The FTIR analysis showed all typical absorption characteristics of HAp. However, some carbonate content was observed around 870 and 1664 cm^{-1}, which are indications for the presence of carbonated apatite along with pure apatite [35–38].

4. Conclusion

In summary, BG-based composites reinforced by 0, 10, 20 and 30 wt% of NF nanoparticles were fabricated by cold pressing method based on hybrid microstructure design. Significant improvements in fracture toughness have been attributed to the synergetic effects of NF. Addition of NF can be used successfully to improve the toughening properties of the composites without affecting other intrinsic properties such as bioactivity. In addition, the experiments provide data to support the use of the nanocomposite in bone repair applications. This is a preliminary study, and more detailed work is required to evaluate other properties of the hybrid nanocomposites.

References

[1] K. Niihara, New design concept of structural ceramics–ceramic nanocomposites, J. Ceram. Soc. Jpn. (Int. Ed). 99 (1991) 945–952.
[2] L.L. Hench, The challenge of orthopaedic materials, Curr. Orthopaed. 14 (2000) 7.
[3] L.L. Hench, in: T. Yamamuro, L.L. Hench, J. Wilson (Eds.), Handbook of Bioactive Ceramics, vol. 1, CRC, Press, Boca Raton, 1990, p. 7.
[4] H. Ylanen, K.H. Karlsson, A. Itala, H.T. Aro, Effect of immersion in SBF on porous bioactive bodies made by sintering bioactive glass microspheres, J. Non-Cryst. Solids 275 (2000) 107–115.
[5] M. Mozafari, M. Rabiee, M. Azami, S. Maleknia, Biomimetic formation of apatite on the surface of porous gelatin/bioactive glass nanocomposite scaffolds, Appl. Surf. Sci. 257 (2010) 1740–1749.

[6] A. Hamlekhan, M. Mozafari, N. Nezafati, M. Azami, H. Hadipour, A proposed fabrication method of novel PCL-GEL-HAp nanocomposite scaffolds for bone tissue engineering applications, Adv. Compos. Lett. 19 (2010) 123–130.
[7] J. Alkemper, H. Fuess, Devitrification of bioactive invert phosphate glasses, J. Non-Cryst. Solids 210 (1997) 32–40.
[8] M. Mozafari, F. Moztarzadeh, Novel porous gelatin/bioactive glass scaffolds with controlled pore structure engineered via compound techniques for bone tissue engineering, in: 1st Middle East Conference on Biomedical Engineering (IEEE), 2011, Sharjah, UAE., (2011), pp. 104–107. , doi:10.1109/MECBME.2011.5752076.
[9] S. Taherkhani, F. Moztarzadeh, M. Mozafari, Sol–gel synthesis and characterization of unexpected rod-like crystal fibers based on SiO_2–$(1-x)CaO-xSrO$–P_2O_5 dried-gel, J. Non-Cryst. Solids 358 (2012) 342–348.
[10] A. Sepahvandi, F. Moztarzadeh, M. Mozafari, M. Ghaffari, N. Raee, Photoluminescence in the characterization and early detection of biomimetic bone-like apatite formation on the surface of alkaline-treated titanium implant: state of the art, Colloids Surf. B: Biointerfaces 86 (2011) 390–396.
[11] A. Hamlekhan, F. Moztarzadeh, M. Mozafari, M. Azami, N. Nezafati, Preparation of laminated poly((-caprolactone)-gelatin-hydroxyapatite nanocomposite scaffold bioengineered via compound techniques for bone substitution, Biomatter 1 (2011) 1–11.
[12] N. Nezafati, F. Moztarzadeh, S. Hesaraki, M. Mozafari, A. Samadikuchaksaraei, L. Hajibaki, M. Gholipour, Effect of silver concentration on bioactivity and antibacterial properties of SiO_2–CaO–P_2O_5–Ag_2O sol–gel derived bioactive glass, Key Eng. Mater. 493–494 (2012) 74–79.
[13] T. Kokubo, Novel bioactive materials, Anal. Quim. Int. Ed. 93 (1997) S49.
[14] C.T. Wu, J. Chang, Synthesis, Apatite-formation ability of akermanite, Mater. Lett. 58 (2004) 2415–2417.
[15] S. Ni, L. Chou, J. Chang, Preparation and characterization of forsterite (Mg_2SiO_4) bioceramics, Ceram. Int. 33 (2007) 83–88.
[16] S. Ni, L. Chou, J. Chang, In vitro studies of novel CaO–SiO_2–MgO system composite bioceramics, J. Mater. Sci. Mater. Med. 19 (2008) 359–367.
[17] B.D. Cullity, Elements of X-ray Diffraction, Prentice Hall, Addison-Wesley, 1978.
[18] L.G. Gutwein, T.J. Webster, Osteoblast and chrondrocyte proliferation in the presence of alumina and titania nanoparticles, J. Nanoparticle Res. 4 (2002) 231–238.
[19] A. Ghosh, A.K. Suri, B.T. Rao, T.R. Ramamohan, Low-temperature sintering and mechanical property evaluation of nanocrystalline 8 mol% yttria fully stabilized zirconia, J. Am. Ceram. Soc. 90 (2007) 2015–2023.
[20] C. Du, F.Z. Cui, X.D. Zhu, Kde Groot, Three-dimensional nano-HAp/collagen matrix loading with osteogenic cells in organ culture, J. Biomed. Mater. Res. 44 (1999) 407–415.
[21] N. Nezafati, F. Moztarzadeh, S. Hesaraki, M. Mozafari, Synergistically reinforcement of a self-setting calcium phosphate cement with bioactive glass fibers, Ceram. Int. 37 (2010) 927–934.
[22] N. Nezafati, F. Moztarzadeh, M. Mozafari, In vitro evaluations of a mechanically optimized calcium phosphate cement as a filler for bone repair, Key Eng. Mater. 493–494 (2012) 209–214.
[23] M. Vallet-Regi, Ceramics for medical applications, J. Chem. Soc. Dalton Trans. 2 (2001) 97.
[24] J.Y. Chen, Y.R. Duan, C.L. Deng, Q.Y. Zhang, X.D. Zhang, A comparative study between dynamic and static simulated body fluid methods, in: Bioceramics 18 (vols. 309–311), Key Engineering Materials, 2006.
[25] M.H. Fathi, M. Kharaziha, Two-step sintering of dense, nanostructural forsterite, Mater. Lett. 63 (2009) 1455–1458.
[26] A. Razavi, F. Moztarzadeh, M. Mozafari, M. Azami, F. Baghbani, Synthesis and characterization of high-pure nanocrystalline forsterite and its potential for soft tissue applications, Adv. Compos. Lett. 20 (2011) 41–47.
[27] R. Ravarian, F. Moztarzadeh, M. Solati Hashjin, S.M. Rabiee, P. Khoshakhlagh, M. Tahriri, Synthesis, characterization and bioactivity investigation of bioglass/hydroxyapatite composite, Ceram. Int. 36 (2010) 291–297.
[28] H. Yang, C.T. Prewitt, On the crystal structure of pseudowollastonite ($CaSiO_3$), Am. Miner. 84 (1999) 929–932.
[29] M. Azami, S. Jalilifiroozinezhad, M. Mozafari, Synthesis and solubility of calcium fluoride/hydroxy-fluorapatite nanocrystals for dental applications, Ceram. Int. 37 (2011) 2007–2014.
[30] J. Lambers, P. Hess, Infrared spectra of photochemically grown suboxides at the SiO/SiO_2 interface, J. Appl. Phys. 94 (2003) 2937–2941.
[31] T.S. Duffy, C.S. Zha, R.T. Downs, H.K. Mao, R.J. Hemley, Elasticity of forsterite to 16 GPa and the composition of the upper mantle, Nature 378 (1995) 170–173.
[32] E. Libowitzky, A. Beran, OH defects in forsterite, Phys. Chem. Miner. 22 (1999) 387–392.
[33] S.A. Poursamar, M. Azami, M. Mozafari, Controllable synthesis and characterization of porous polyvinyl alcohol/hydroxyapatite nanocomposite scaffolds via an in situ colloidal technique, Colloids Surf. B: Biointerfaces 84 (2011) 310–316.
[34] A. Hamlehkhan, M. Mozafari, N. Nezafati, M. Azami, A. Samadikuchaksaraei, Novel bioactive poly((-caprolactone)-gelatin-hydroxyapatite nanocomposite scaffolds for bone regeneration, Key Eng. Mater. 493–494 (2012) 909–915.
[35] A. Ghafari Nazari, A. Tahari, F. Moztarzadeh, M. Mozafari, M.E. Bahrololoom, Ion exchange behavior of silver doped apatite micro and nano particles as antibacterial biomaterial, Micro Nano Lett. 6 (2011) 713–717.
[36] C. Du, F.Z. Cui, X.D. Zhu, Kde Groot, Three-dimensional nano-HAp/collagen matrix loading with osteogenic cells in organ culture, J. Biomed. Mater. Res. 44 (1999) 407–415.
[37] M. Azami, S. Jalilifiroozinezhad, M. Mozafari, Calcium fluoride/hydroxyfluorapatite nanocrystals as novel biphasic solid solution for tooth tissue engineering and regenerative dentistry, Key Eng. Mater. 493-494 (2012) 626–631.
[38] S.N. Salama, H.A. El-Batal, Microhardness of phosphate glasses, J. Non-Cryst. Solids 168 (1994) 179–185.